# High-Optical-Power, Wideband Distributed Photodetectors for Optical RF Interconnects



*June 8, 1998*

*Sponsored by*

*Defense Advanced Research Projects Agency (DOD)*

*Electronic Technology Office (ETO)*

*ARPA Order No. D611 Amdt 27*

*Issued by U.S. Army Aviation and Missile Command Under*
*Contract DAAH01-98-C-R017*

*Principal Investigator: Robert A. Marsland*
*Focused Research, Inc.*
*555 Science Dr.*
*Madison, WI 53711*
*608-238-2455*



*Contract sequence number for this data item: A002 on DD Form 1423*

# REPORT DOCUMENTATION PAGE

*Form Approved*
*OMB NO. 0704-0188*



| 1. AGENCY USE ONLY ( Leave Blank) | 2. REPORT DATE | 3. REPORT TYPE AND DATES COVERED |
|---|---|---|
| | July 1998 | Final Report |

**4. TITLE AND SUBTITLE**

High-Optical-Power, Wideband Distributed Photodetectors for Optical RF Interconnects

**5. FUNDING NUMBERS**

C - DAAH01-98-C-R017

**6. AUTHOR(S)**

Robert A. Marsland

**7. PERFORMING ORGANIZATION NAME(S) AND ADDRESS(ES)**

Focused Research, Inc.
555 Science Drive, Suite E
Madison, WI 53711

**8. PERFORMING ORGANIZATION REPORT NUMBER**

FRI 0002

**9. SPONSORING / MONITORING AGENCY NAME(S) AND ADDRESS(ES)**

DARPA/ETO
3701 North Fairfax Drive
Arlington, VA 22203-1704
Bob Leheny

**10. SPONSORING / MONITORING AGENCY REPORT NUMBER**

CLIN 0001AB
DI-MISC-80711
(Sequence A002 of DD1423)

**11. SUPPLEMENTARY NOTES**

**12 a. DISTRIBUTION / AVAILABILITY STATEMENT**

Approved for public release; distribution unlimited

**12 b. DISTRIBUTION CODE**

**13. ABSTRACT (Maximum 200 words)**

We present the results of our Phase I Small Business Innovative Research program to investigate the feasibility of a Schottky-diode based Velocity Matched Distributed Photodetector (VMDP). The goal of the two-phase program is to define a process for designing and fabricating VMDP that achieve >60 GHz bandwidth, >100mA current handling, and >50% efficiency. In this program we designed and fabricated the first devices of this kind. The bandwidth of these first devices was limited to 22 GHz by excessive ohmic resistance. We believe that 100 GHz can be achieved through improved photodiode design. The responsivity of the devices was 0.05A/W limited by poor wafer cleaves and fiber coupling efficiency. Fiber coupling efficiency can be increased through improved waveguide design. A significant output of this program is a method for designing VMDP structures that do not require back-termination. Elimination of the termination resistance doubles efficiency and improves the noise figure. SPICE models were developed to aid in rapid analysis of future designs. We conclude that through improved optical waveguide design and fabrication, it will be feasible to develop devices that meet our original targets.

**14. SUBJECT TERMS**

Velocity matched distributed photodetector, VMDP, Schottky photodiode, high-power photodiode, ridge waveguide.

**15. NUMBER OF PAGES**

v + 28

**16. PRICE CODE**

| 17. SECURITY CLASSIFICATION | 18. SECURITY CLASSIFICATION ON THIS PAGE | 19. SECURITY CLASSIFICATION OF ABSTRACT | 20. LIMITATION OF ABSTRACT |
|---|---|---|---|
| UNCLASSIFIED | UNCLASSIFIED | UNCLASSIFIED | UL |

# Abstract

We present the results of our Phase I Small Business Innovative Research program to investigate the feasibility of a Schottky-diode based Velocity Matched Distributed Photodetector (VMDP). The goal of the two-phase program is to define a process for designing and fabricating VMDP that achieve >60 GHz bandwidth, >100mA current handling, and >50% efficiency. In this program we designed and fabricated the first devices of this kind. The bandwidth of these first devices was limited to 22 GHz by excessive ohmic resistance. We believe that 100 GHz can be achieved through improved photodiode design. The responsivity of the devices was 0.05A/W, limited by poor wafer cleaves and fiber coupling efficiency. Fiber coupling efficiency can be increased through improved waveguide design. A significant output of this program is a method for designing VMDP structures that do not require back-termination. Elimination of the termination resistance doubles efficiency and improves the noise figure. SPICE models were developed to aid in rapid analysis of future designs. We conclude that through improved optical waveguide design and fabrication, it will be feasible to develop devices that meet our original targets.

# Contents


CONTENTS ..... III

FIGURES AND TABLES ..... IV

PREFACE AND ACKNOWLEDGMENTS ..... V

SUMMARY ..... 1

INTRODUCTION ..... 2

METHODS, ASSUMPTIONS, AND PROCEDURES ..... 3
- Designs and Analytical Models ..... 3
- Establishment of Fabrication Process ..... 4
- Verification of Analytical Model ..... 4
- Measurement of Integrated Photodetector ..... 5
- Measure New Focus Diode Saturation ..... 6
- Measure Electrical Waveguide Properties ..... 6
- Design New Electrical Waveguide ..... 7

RESULTS AND DISCUSSION ..... 8
- Designs and Analytical Models ..... 8
- Verification of Analytical Model ..... 15
- Measurement of Integrated Photodetector ..... 18
- Measure New Focus Diode Saturation ..... 21
- Measure Electrical Waveguide Properties ..... 22
- Design New Electrical Waveguide ..... 22

RECOMMENDATIONS ..... 28

REFERENCES ..... 28

# Figures and Tables

Figure 1: Cross-sectional drawing of the New Focus, Inc. photodetector. ..... 3
Figure 2: Design for the Schottky photodetector approach ..... 4
Figure 3: Schematic representation of waveguide test structure ..... 5
Figure 4: Test structures for electrical waveguide measurement ..... 6
Figure 5: Cross section layer structure for the VMDP ..... 8
Figure 6: Preliminary layout of VMDP unit cell for electrical model ..... 8
Figure 7: Electrical model for the Schottky photodiodes used in the VMDP structure ..... 9
Figure 8 : Simulation of Schottky VMDP design using UCLA computer code ..... 10
Figure 9 : Velocity matching of the optical and electrical waves ..... 10
Figure 10: Field profiles for the optical waveguide between and under photodiodes ..... 11
Figure 11 : Simulated optical power in the optical waveguide as a function of distance ..... 11
Figure 12: Final composition of the VMDP structure. ..... 12
Figure 13 : Unit cell of test structure for optical waveguide evaluation ..... 13
Figure 14 : VMDP unit cell version 1 ..... 14
Figure 15 : VMDP unit cell version 2 ..... 14
Figure 16 : VMDP unit cell version 3 ..... 14
Figure 17 : VMDP unit cell version 4 ..... 14
Figure 18 : Complete reticle for the VMDP mask set ..... 16
Figure 20 : Response of the New Focus model 1014 and the VMDP photodiode to the PSP30K laser ..... 19
Figure 21 : Impulse response of single diode in a 7-diode VMDP ..... 20
Figure 22 : Frequency response of the VMDP sample measured by optical heterodyne technique ..... 21
Figure 23 : Electrical transmission line loss ..... 21
Figure 24 : Layout of test structure to evaluate effect of doped strip of semiconductor ..... 22
Figure 25 : Illustration of how current sources can be connected to an unterminated transmission line ... 23
Figure 26 : Simple model to test Ginzton approach to no termination on distrubuted current source line. 25
Figure 27 : Four diode unterminated VMDP structure used in simulations ..... 25
Figure 28 : Frequency response of a uniform VMDP with no input termination ..... 26
Figure 29 : Step response of the unterminated uniform VMDP structure ..... 26
Figure 30 : Frequency reponse of the unterminated VMDP using the Ginzton approach ..... 27
Figure 31 : Step response of the unterminated VMDP using backward-wave cancelation. ..... 27

Table 1 : Target characteristics for VMDP devices at the end of Phase II ..... 2
Table 2 : Summary of VMDP design and process variations ..... 13
Table 3 : Sumary of insertion-loss data for the various waveguide test structures. ..... 17
Table 4 : Summary of waveguide parameters. ..... 18

# Preface and Acknowledgments

Prof. Wu's group at UCLA collaborated in this work while continuing to pursue the MSM approach under a separate program. Our efforts focused on the Schottky approach, but we worked closely with the UCLA group to leverage their efforts and share epitaxial growth runs, reducing cost and lead-time for material. We are particularly indebted to Dr. Al Cho of Lucent Technologies for providing the epitaxial material.

# Summary

In this Phase I program, we set out to show the feasibility of a Schottky-diode based Velocity Matched Distributed Photodetector (VMDP) with greater than 50% efficiency. This photodiode achieves higher power handling capability by combining the outputs of 5 to 10 photodiodes, but does it in such a way that the bandwidth degradation due the cascading does not degrade as rapidly as it would if the diodes were all lumped together. It is quite comparable to a distributed amplifier. Because this is a traveling wave structure, the assumption is that one port of the diode must be terminated resulting in a loss of 50% of the photocurrent. Part of this Phase I program was to challenge that assumption as well.

Since the inception of this idea by Prof. M.C. Wu and T. Itoh at UCLA, the feasibility studies have involved MSM photodiode structures on GaAs. More recently, the UCLA group fabricated an InGaAs metal-semiconductor-metal (MSM) VMDP structure. The conclusion is that the MSM will never provide the power-handling capability that a vertical diode can. However, the vertical diode poses several challenges because of the requirement to make ohmic contact to the lower layers.

This program, which was in collaboration with the UCLA group mentioned above, has achieved the following:

1. First demonstration of integration of Schottky photodiode with optical waveguide,
2. Totally new design approach for VMDP that obviates the need for back termination, doubling efficiency and improving noise figure,
3. Easy-to-use Spice model for designing VMDP structures.

These accomplishments clear the way to a focused program to fully define the fabrication and design processes. The following work remains before efficient 100 mA, >60 GHz detectors can be commercialized:

1. An optical waveguide must be designed that achieves 90% fiber coupling efficiency,
2. Photodiode undercut during the mesa and ridge etches must be eliminated,
3. Optical waveguide losses must be reduced.

We have plans for each of the above tasks and look forward to future work on these devices.

# Introduction

The purpose of this Phase I SBIR program was to demonstrate the feasibility of a Schottky-diode based Velocity-Matched-Distributed-Photodetector (VMDP) and to come up with an estimate for eventual device cost. The VMDP is similar to a traveling-wave photodetector, with the important distinction that the photodiode is not fully distributed along the waveguide. It is split into discrete detectors to facilitate velocity matching and power-handling capability. We expected that the Schottky design would have superior saturation performance and power-handling ability compared to the Metal-Semiconductor-Metal (MSM) VMDP approach pursued to date. We also anticipated that greater than 50% quantum efficiency could be achieved over a band of frequencies by analogy to the distributed amplifier. Our target characteristics for the end of a Phase II follow-on are summarized in Table 1.

*Table 1 : Target characteristics for VMDP devices at the end of Phase II*

| *Characteristic:* | *Value:* |
|---|---|
| Responsivity | 0.6 A/W |
| Power Saturation (1 dB) | 100 mW |
| Wavelength Range | 1.4 to 1.6 μm |
| Input Fiber | SMF-28 fiber |
| Output Connector | 1.85 mm "V" |
| Bias Voltage | 4.5 V |
| Frequency Response | dc to > 60 GHz |

Prof. Wu's group at UCLA has already carried out a detailed design, analysis, and experimental demonstration for the case of an MSM-VMDP on GaAs [1]. The GaAs design employed low-temperature-grown (LT) GaAs as the absorbing layer and 0.3 μm wide electrodes with 0.2 μm spacing to form the MSM detector elements. Showing InP-based design feasibility was the main goal of this program of research. The InP version is different from the GaAs version in the following respects:

1. The absorbing material must be InGaAs for 1.55 μm operation. The low-temperature growth advantages have not been shown for InGaAs,
2. The low band-gap and Schottky barrier height of InGaAs requires a barrier enhancement layer and special care to avoid leakage and device failure at the etched mesa edge,
3. An InP-based design will involve different materials and processing methods,
4. We wish to eliminate the sub-micron lithography and leverage the existing New Focus InP-based Schottky photodetector design,
5. A Schottky diode design requires an N+ cathode layer which introduces additional electrical and optical loss as well as requiring an additional etch step,
6. A Schottky diode design requires separate anode and cathode contact metallization.

# Methods, Assumptions, and Procedures

*Designs and Analytical Models*

The design approach was to stick to the New Focus InGaAs/InP photodiode process as much as possible while incorporating the optical waveguide and electrical transmission line. A cross-section of the New Focus InGaAs/InP Schottky photodiode is shown in Figure 1. A self-aligned wet etch and Gold-Germanium/ Nickel/ Gold (AuGe/Ni/Au) deposition forms the ohmic contact to the underlying N+ layer. A wet-etch down to the semi-insulating InP substrate isolates the diode layers from the bonding pads. A multi-layer Titanium/ Platinum/ Gold (Ti/Pt/Au) metal scheme forms the Schottky contact and bond pads simultaneously. A plated air-bridge structure connects the Schottky contact with the bond-pad to avoid issues of step-coverage and extra capacitance or shorting to the photodiode layers.

Starting with this process, we needed to design an optical waveguide into this same cross-section for propagation normal to the page. The optical waveguide layers can't be inserted into the undoped region of the diode because the increase in transit time would be unacceptable, nor could the layers be inserted into the N+ layer because the optical losses would be unacceptable. The only direct approach was to place the optical waveguide below the N+ layer. The need for keeping the optical field away from the N+ layer as much as possible and the need to couple through the N+ layer to reach the absorbing region put strict limits on the maximum thickness of the N+ layer. However, a thick N+ layer is desirable for low diode series resistance. The UCLA group analyzed this trade-off using the beam propagation method (BPM) to model the optical losses and discontinuities, and their own code for modeling the electrical waveguide performance.

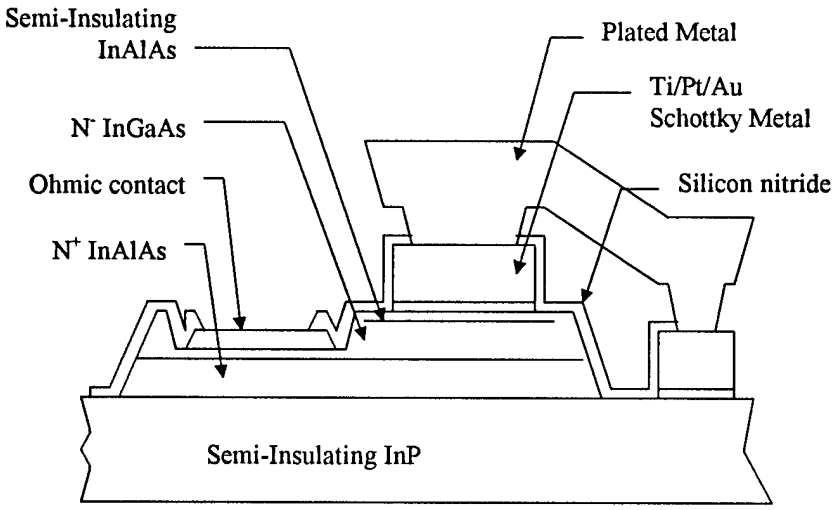


*Figure 1: Cross-sectional drawing of the New Focus, Inc. photodetector.*

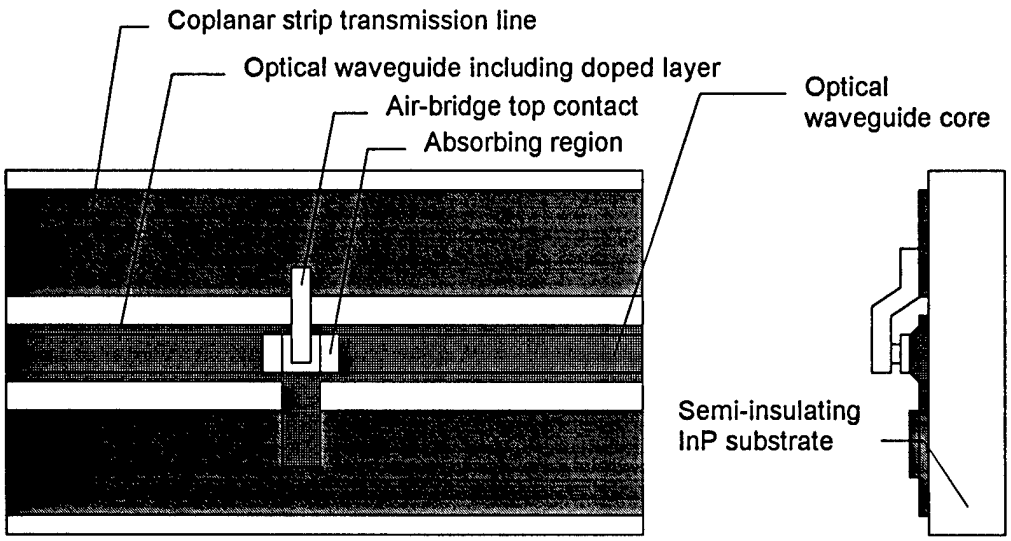


*Figure 2: Design for the Schottky photodetector approach showing one detecting element section (left) and a cross-section through the diode (right).*

### *Establishment of Fabrication Process*

The starting point for the fabrication process was our existing process for making single-element Schottky diodes for New Focus, Inc. This process had to be modified in two ways. First, the isolation etch for the photodiode can't go all the way to the InP substrate without destroying the waveguides, so the photodiodes were isolated by removing only the top layers and leaving the lower N+ layer. Second, an etch step was added to define the ridge for the optical waveguide. The mesa etch is critical in that it must stop on top of the top optical waveguide cladding layer and form a smooth, flat surface to minimize scattering loss in the optical waveguide. Fortunately, the UCLA group had already worked out this problem by the time we got to it. A mixture of 1g anhydrous citric acid to 1ml de-ionized water mixed 0.5:1 with ammonium hydroxide provides 17Å/s on InGaAs and 0.5Å/s on InAlAs.

### *Verification of Analytical Model*

From work in the field of opto-electronic integrated circuits (OEICs) for 1.55 μm light-emission and switching, the optical properties and processing methods for InP-based optical circuits have been fairly well defined [2]. However, most of this work involves P-I-N structures and has shown substantial polarization dependent loss primarily due to the heavily doped P-type region. Also, the VMDP design involves multiple active-passive waveguide transitions that have not been extensively studied in the InP system.

Our approach was to fabricate InP-based waveguiding structures for 1.55 μm VMDP operation and characterize the active-passive waveguide discontinuity and waveguide polarization-dependent loss. The experimental approach is to use test structures represented schematically in Figure 3. Waveguides A, B, and C have the same amount of active (absorbing) material but varying numbers of transitions. The slope of the waveguide total insertion loss (in dB) versus the number of transitions provides the transition loss. Waveguides D, E, and F have the same number of transitions, but varying amounts of

active waveguide. The slope of the waveguide total insertion loss (in dB) versus length of active material provides the difference between the active and passive waveguide loss. We assumed that coupling efficiency would vary randomly and not substantially between the waveguides so that this effect could be averaged out over multiple test structures.

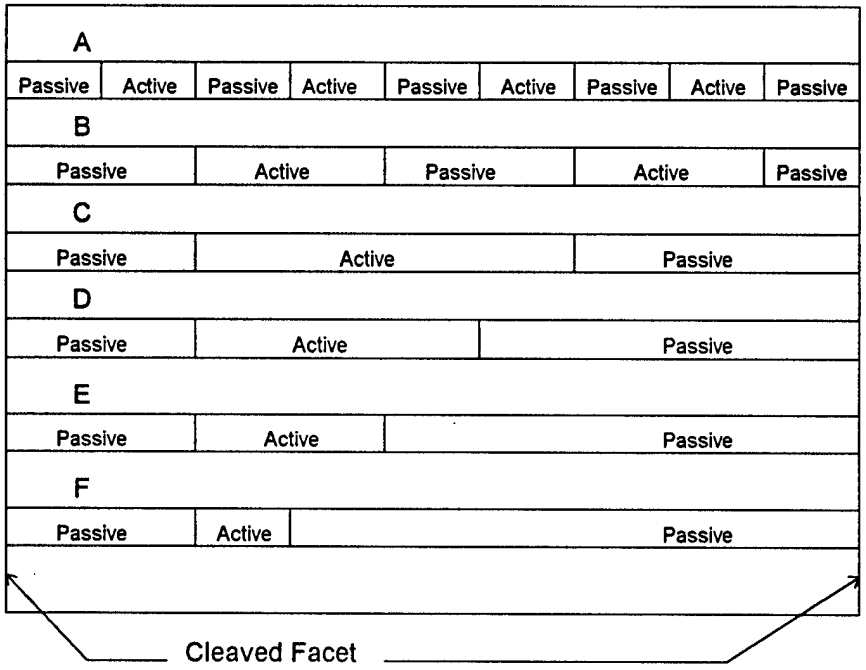


*Figure 3: Schematic representation of waveguide test structure for separately determining active and passive waveguide loss and active to passive waveguide coupling.*

### *Measurement of Integrated Photodetector*

The integration of the photodetector with the optical waveguide such that their performance is not degraded is the primary risk in this technology. The impact of the restrictions of the optical waveguide design on the photodetector is assessed in this task.

In the UCLA GaAs VMDP effort, the approach was to fabricate complete VMDP structures with varying numbers of photodetector elements to allow simultaneous measurement of waveguide and photodetector performance [1]. However, this requires high detector element yield to eliminate the confusion that would result from mixtures of good and bad detectors in the various samples. Given the short duration of the Phase I effort, we took an approach that would produce useful information on photodetector performance so long as a single photodetector / waveguide combination can be made to function. This approach required waveguide properties to be known to sufficient accuracy to allow the internal performance of the photodetector to be calculated.

We fabricated single-element VMDP structures with varying diode (active waveguide) length and calculated photodetector saturation and responsivity. It is important to have a diode length that is sufficient to allow AC saturation at the power levels we will be able to couple into the optical waveguide.

Saturation measurements were performed with the large-signal, time-domain technique using 50 ps pulses at 1.55 μm with power levels up to 100 mW. The 50 ps pulse-width is set by the Optoelectronics Inc. PPL30K laser system and is perfectly adequate for saturation measurements.

### *Measure New Focus Diode Saturation*

For comparison and to establish the characterization set-up, we measured the saturation characteristics of the existing New Focus InP-based photodetector. We expected these saturation characteristics to be very similar to the single-element saturation characteristics of the VMDP. Any differences indicate that the device changes imposed by the waveguide have altered the performance of the photodetector. For example, layout and free-carrier absorption concerns could lead to a structure with higher series resistance, which would reduce the saturation power. The method used for this test is identical to that used for the integrated photodiode test, which avoids difficulties in comparing techniques or interpreting results. This is particularly important given that we are using a pulsed laser to measure saturation. Pulse properties affect the saturation level and make comparisons between different laser sources difficult.

### *Measure Electrical Waveguide Properties*

Here we evaluate the impact of the photodetector's doped layer on the electrical waveguide. The electrical wave propagating down the coplanar transmission line induces a current in the adjacent doped region (see Figure 2) that results in electrical power loss and dispersion. We measured electrical waveguides with and without the photodetector layers being etched away. These electrical waveguides were designed to be 50 ohms without photodetector loading and no photodetector connections will be made. The measurement is made by on-wafer probing and vector-network-analysis through collaboration with the UCLA group. An example of the proposed test structure and measurement is shown in Figure 4.

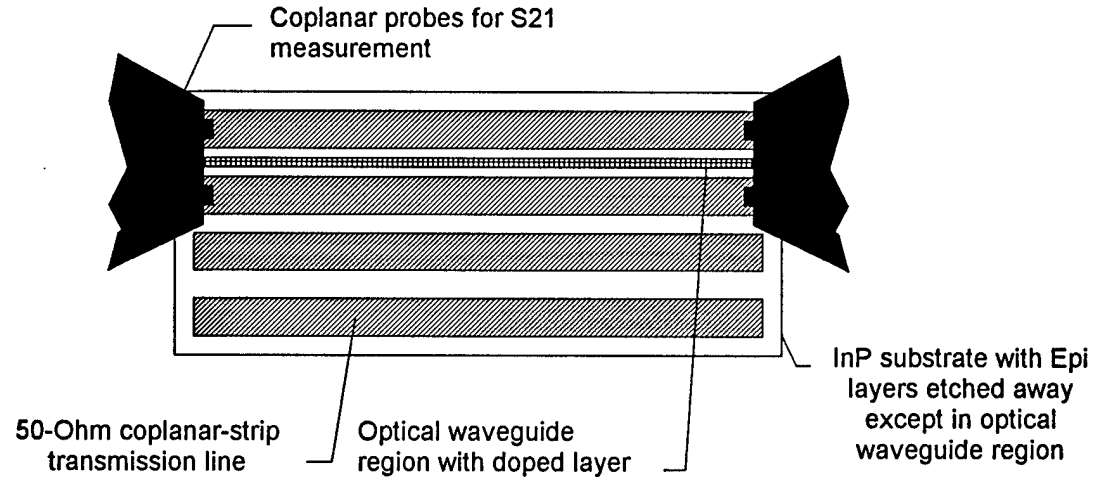


*Figure 4: Test structures for electrical waveguide measurement will include 50 ohms coplanar lines with and without the doped layer in the optical waveguide etched away.*

*Design New Electrical Waveguide*

Once the photodetector and waveguide performance and fabrication methods are established, the primary design challenge is velocity matching between the optical and electrical waves on the VMDP. The experience of the UCLA group gives us confidence that this is a matter of design and development, not a major feasibility issue. However, there is another electrical waveguide design issue that could effect the acceptance of these devices into low-noise RF applications: back termination. The noise generated by the back-termination resistor is not a major concern in high-optical-power systems (since shot-noise dominates), but the fact that half the signal is lost could be a factor.

We investigated via computer simulation with MicroSim PSpice various methods for achieving cancellation of the backward traveling waves and a consequent doubling in signal amplitude in the forward direction.

# Results and Discussion

### *Designs and Analytical Models*

Given the constraints described previously, the layer structure needed to be as shown in Figure 5. The primary design tasks were to decide what material composition to use for the various layers and what to do with the layer labeled "transparent $n^+$" since its thickness affects both optical and electrical properties. Based on the preliminary physical layout shown in Figure 6 we developed a simple electrical model that would allow quick analysis of the impact of various layer thicknesses.

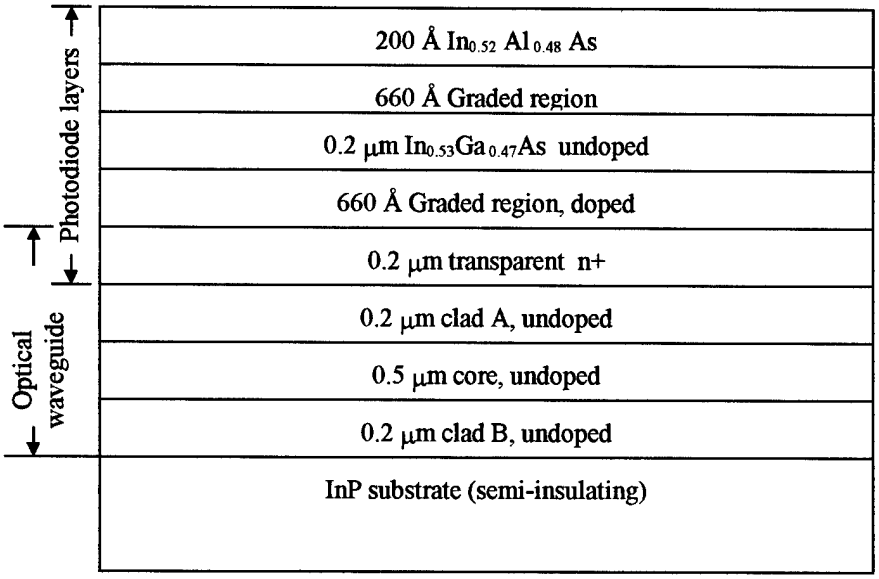


*Figure 5: Cross section layer structure for the VMDP.*

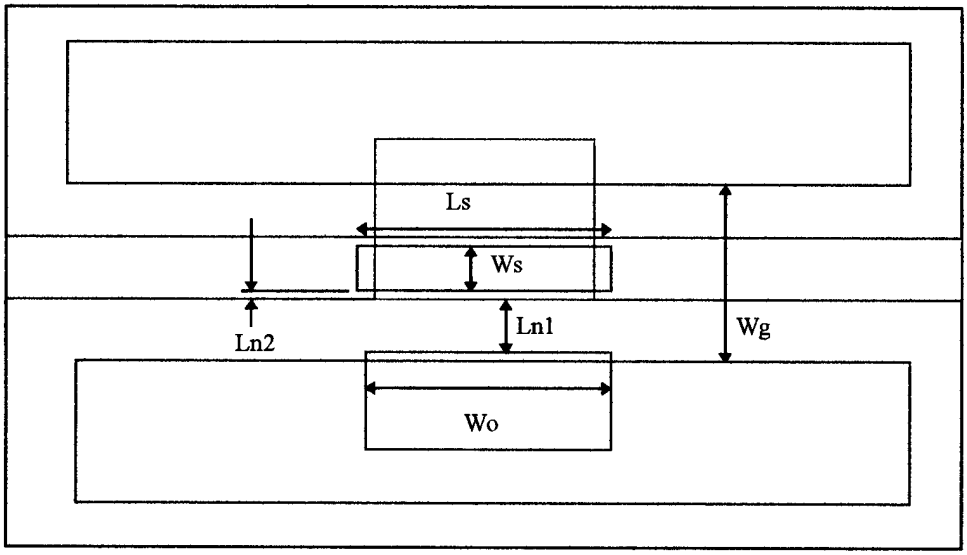


*Figure 6: Preliminary layout of VMDP unit cell for electrical model.*

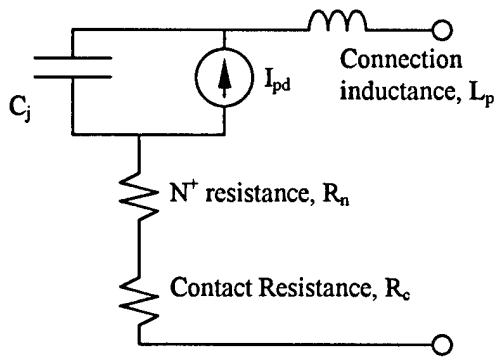


*Figure 7: Electrical model for the Schottky photodiodes used in the VMDP structure.*

**Model parameters:**

$W_s$ = width of Schottky contact
$L_s$ = length of Schottky contact
$L_n$ = separation between Schottky and ohmic
$W_o$ = width of ohmic
$d_i, d_{n1}, d_{n2}$ = thickness of depleted region under Schottky, n+ thickness outside of ridge, $n^+$ thickness under ridge
$r_c$ = contact resistance per unit width
$R_{sq}$ = $n^+$ sheet resistance per square (thickness divided by resistivity as grown )

**Equations:**

$$R_C = r_c / W_o$$

$$R_n = R_{sq}\left(\frac{L_{n1}}{W_o}\frac{d_{n2}}{d_{n1}} + \frac{L_{n2}}{W_o} + \frac{W_s}{2L_s}\right)$$

$$C_j = \varepsilon\left(\frac{L_s W_s}{d_i}\right) * 1.2$$ ; fudge factor for fringe-field capacitance

$L_p$ = neglected for Wg < 100 μm.

Typical numbers for InAlAs $n^+$:
$R_{sq} = 8/d_{n2}$ ($d_{n2}$ in microns)
$r_c$ = 0.04 ohm-millimeters

Using the following set of parameters,

$$W_s = 2\mu m,\ L_s = 20\mu m,\ L_{n1} = 2\mu m,\ L_{n2} = 1\mu m,\ W_o = 36\mu m$$

for the diode layout and

$$d_i = 0.286\mu m,\ d_{n1} = 0.2\mu m,\ d_{n2} = 0.1\mu m,$$

for the epitaxial layers we found acceptable diode and waveguide properties. The resulting diode parameters are:

$$C_j = \varepsilon \frac{L_s W_s}{d_i} = 21\text{fF},\ R_n = R_{sq}\left(\frac{L_{n1}}{W_o}\frac{d_{n2}}{d_{n1}} + \frac{L_{n2}}{W_o} + \frac{W_s}{2L_s}\right) = 7.56,\ R_c = {}^{0.04}\!/_{W_o} = 1.11\Omega$$

Using these parameters and the previously developed computer code, the UCLA group predicted the microwave performance shown in Figure 8 after achieving velocity match between the electrical and optical waves. The results of the waveguide optimization are shown in Figure 9.

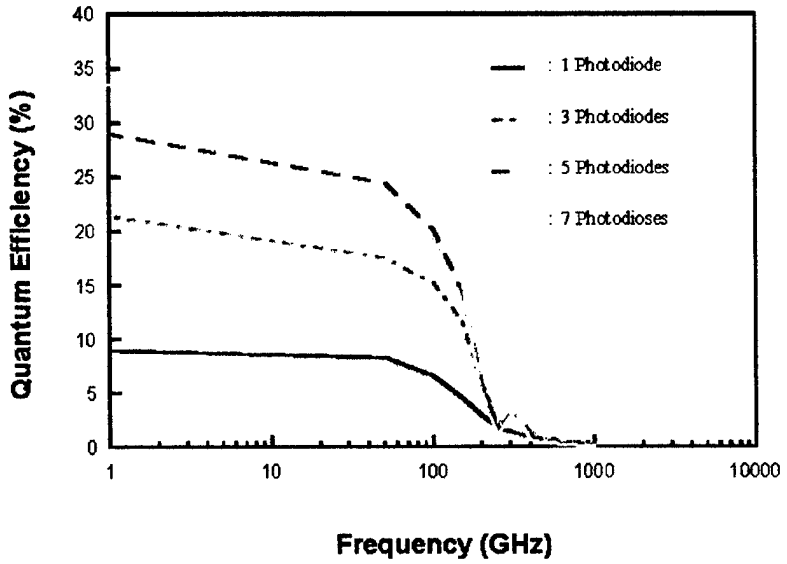


*Figure 8 : Simulation of Schottky VMDP design using UCLA computer code and model parameters above.*

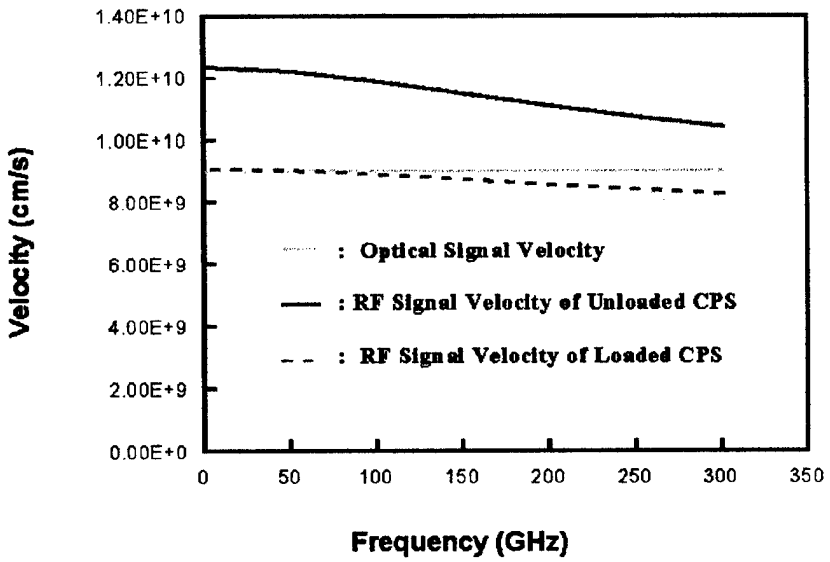


*Figure 9 : The velocity of the optical and electrical waves is matched by adjusting the unloaded CPS geometry and the diode capacitance.*

The Beam Propagation Method (BPM) was used to analyze the resulting optical waveguide structure and discontinuities at the photodiode. The resulting optical field

profiles are shown in Figure 10. The calculations show that the extra ridge height provided by the photodiode increases the lateral confinement and decreases the lateral mode size under the photodiode. This creates an optical discontinuity.

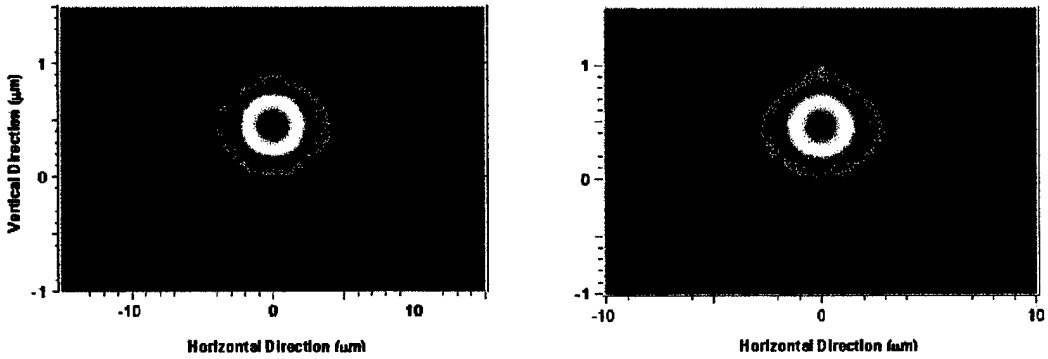


*Figure 10: Field profiles for the optical waveguide between photodiodes (left) and under a photodiode (right). The extra height of the photodiode increases the lateral optical confinement. Note different scales on the various axes.*

The effect of absorption in the photodiode, modal mismatch between the photodiode and the optical waveguide, and free carrier absorption can be seen in Figure 11. The 17% loss per diode is primarily photodiode absorption. The 5% loss between diodes is believed to be the effect of scattering from the modal mismatch at the photodiode. The scattered light takes some distance to radiate away from the waveguide. Free carrier absorption in the section between diodes was not a significant factor.

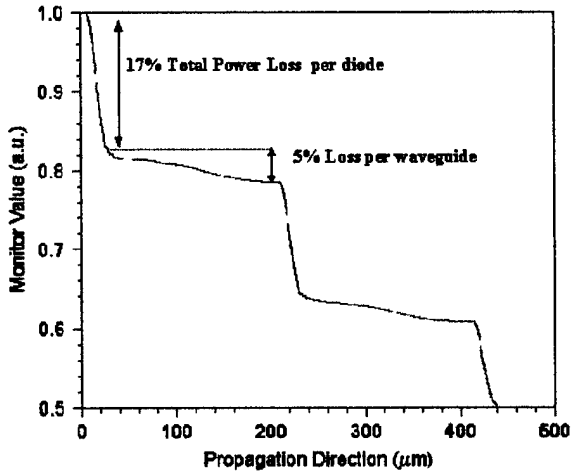


*Figure 11 : Simulated optical power in the optical waveguide as a function of distance along the VMDP. Mode coupling loss, photodiode absorption, and waveguide free carrier absorption are modeled.*

These structures could have been fabricated by either metal-organic chemical-vapor deposition (MOCVD) or molecular-beam epitaxy (MBE). We briefly considered an approach using MOCVD and aluminum-free layers to facilitate re-growth. Re-growing material over the optical waveguide could reduce the optical losses at the photodiode interfaces. However, this approach was too elaborate for a Phase I program. Also, our only source of known high-quality epitaxial material for a structure like this was Dr. Al

Cho at Lucent Technologies who uses MBE. Finally, we wanted to maintain similarity with the New Focus design which uses MBE growth. Because of the difficulty in growing phosphorous-containing materials by MBE, we chose the composition shown in Figure 12. The main difficulties with growing this structure are achieving lattice match and handling two different Gallium compositions. Dr. Al Cho is very experienced with this and was able to produce the material quickly. Our experience is that the commercial epitaxy vendors are very flexible in dealing with these problems, but need at least 6 months to learn how to grow a structure this complex.

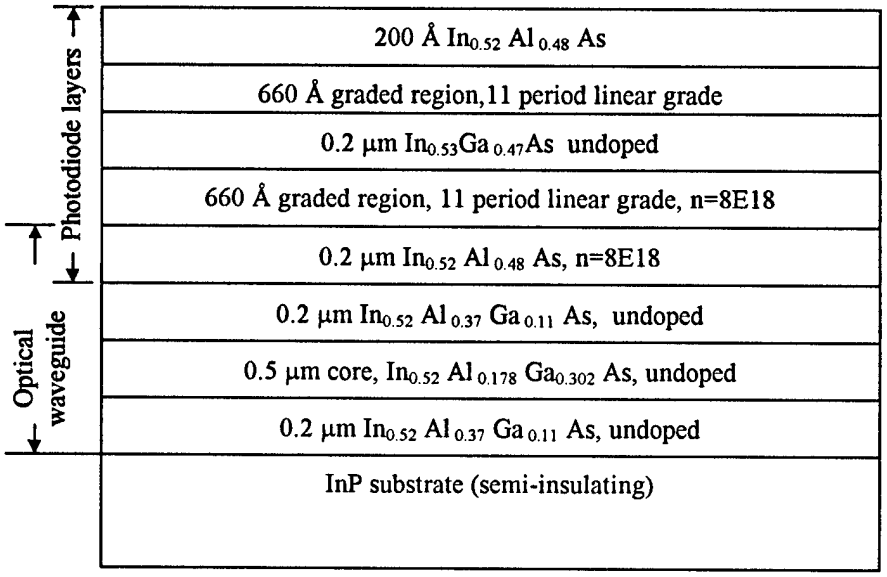


*Figure 12: Final composition of the VMDP structure.*

With the epitaxial structure defined, the next step was to detail the physical layout. We designed four variations of the VMDP and two sets of waveguide test structures. The unit-cell of the test structure for measuring photodiode loss is shown in Figure 13. The same length of active-waveguide sections is included in the top two waveguides, but the lower waveguide has twice as many sections. The relative loss of these two guides will indicate the loss due to passive-active waveguide mode mismatch. The next two waveguides repeat the same experiment with shorter active waveguide. Comparing the relative loss of these two with the previous two will indicate any length-dependent effects in the mode-mismatch loss. The next six waveguides include varying lengths of active waveguide with a constant number of transitions. Comparing the relative loss of these waveguides will provide loss verses unit length of the active waveguide relative to that of the passive waveguide. Completely passive waveguides of varying widths were also included on the mask.

The four variations of VMDP unit cells are shown in Figure 14 through Figure 17. The cells were designed to accommodate three different fabrication approaches and two different ridge widths. Varying fabrication approaches were required because the Schottky contact is so narrow that we were concerned about making air-bridge contact to it. Larger contacts can be used if some material is removed from beneath by etching or using a silicon nitride layer to insulate a portion of the contact from the semiconductor.

The approaches are summarized in Table 2. The only approach completed under this phase of the program was the baseline process. In this process, only designs VMDP2 and VMDP3 will fabricated as designed.

*Table 2 : Summary of VMDP design and process variations*

| Design | Ridge width | Schottky Metal | Note |
|---|---|---|---|
| VMDP1 | 4-μm ridge | 60 $\mu m^2$ | Large Schottky contact used as an etch mask to reduce photodiode area |
| VMDP2 | 4-μm ridge | 40 $\mu m^2$ | Baseline design |
| VMDP3 | 5 μm ridge | 40 $\mu m^2$ | Wider ridge |
| VMDP4 | 4-μm ridge | 84 $\mu m^2$ | Silicon Nitride insulates edges of Schottky contact to reduce photodiode area |

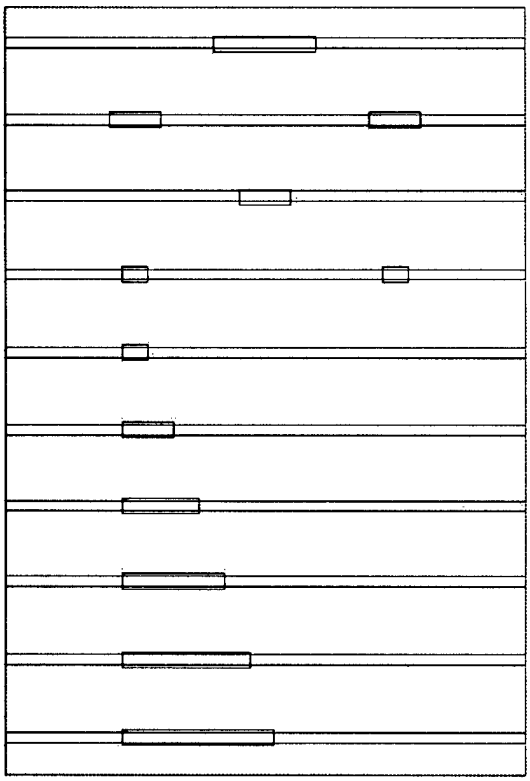

*Figure 13 : Unit cell of test structure for optical waveguide evaluation. The lines extending edge to edge define the ridge of the passive waveguides. The rectangles slightly wider than the waveguide define an active region. The unit cell is repeated 10 times in the complete structure.*

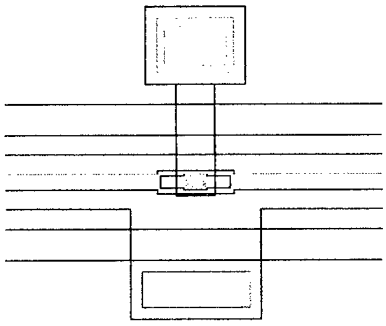

*Figure 14 : VMDP cell version 1. This version has an oversized Schottky contact that can be used as an etch mask for the device isolation step.*

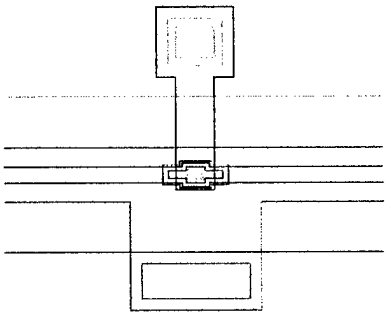

*Figure 15 : VMDP unit cell version 2. This one has the correct area for the Schottky (40 $\mu m^2$) but is shaped to allow more room for the air-bridge connection. The ridge is also widened to allow room for the bridge post area. The Schottky contact is not used as the isolation etch mask here.*

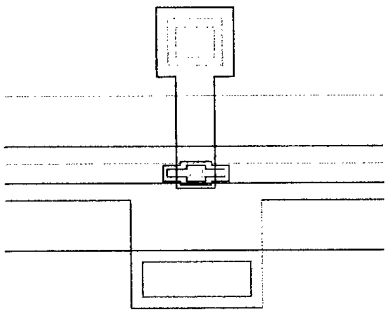

*Figure 16 : VMDP version 3. This version has a wider ridge in case there is an over-etch problem.*

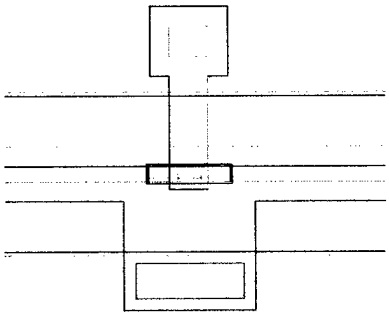

*Figure 17 VMDP version 4. This version has an oversized Schottky contact for high-yield air-bridge connection. Silicon nitride under the edges of the Schottky contact limits the active device area to the correct value.*

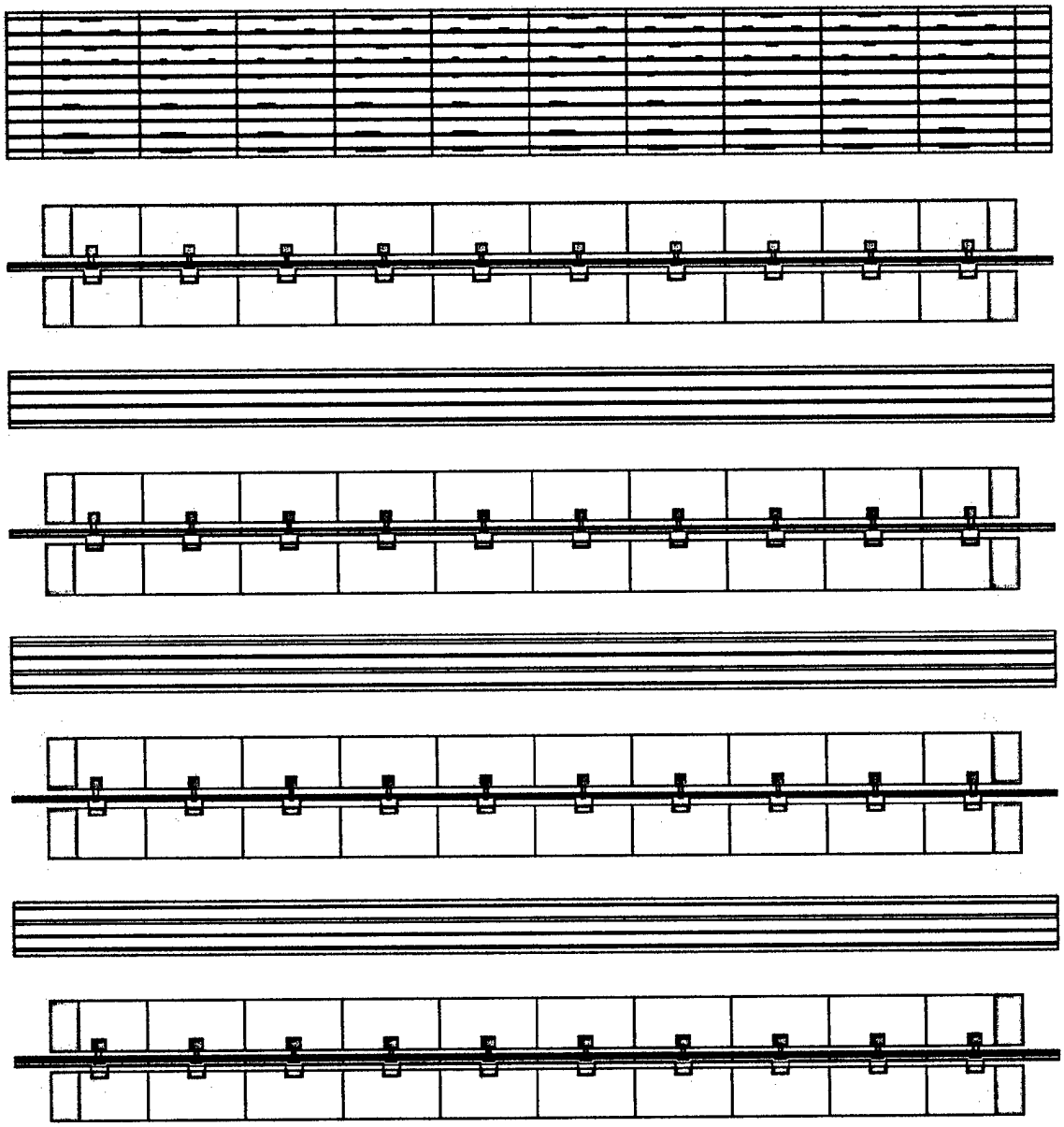

*Figure 18 : Complete reticle for the VMDP mask set. Waveguides are continuous between instances of the reticle on the mask so that cleaves need not be precise in location. The set of four waveguides between each VMDP design are completely passive and have ridge widths of 4, 4.5, 5, and 5.5 μm.*

### *Verification of Analytical Model*

The primary unknowns in the model for the VMDP are the active waveguide loss, passive waveguide loss, and mode-coupling loss between the active and passive guides. To investigate these parameters for our design, we fabricated a piece of the wafer through the first few steps of the process up to the point where the active and passive waveguides were formed but before diodes were contacted. Then we cleaved the piece to form facets for optical coupling. No effort was made to cleave exactly along unit cell lines, so we were left with one piece with 19 unit cells (almost two VMDPs wide as shown in Figure 18) and one with 8 unit cells. We tested the insertion loss of the test structures on each of

these pieces. One of the test structures is described in Figure 13, the other is simply a group of passive waveguides of varying width shown in Figure 18.

The test set-up is described in Figure 19. Although this is a DC measurement, we used the PPL30K pulsed 1.55 μm laser-source obtained for the time-domain measurements since it is the only source we had available at this wavelength. The PPL30K has <1μW average power, so we used an oscilloscope and amplified high-speed detector to view the transmitted pulse. This gave excellent signal-to-noise ratio even for attenuation over 30 dB.

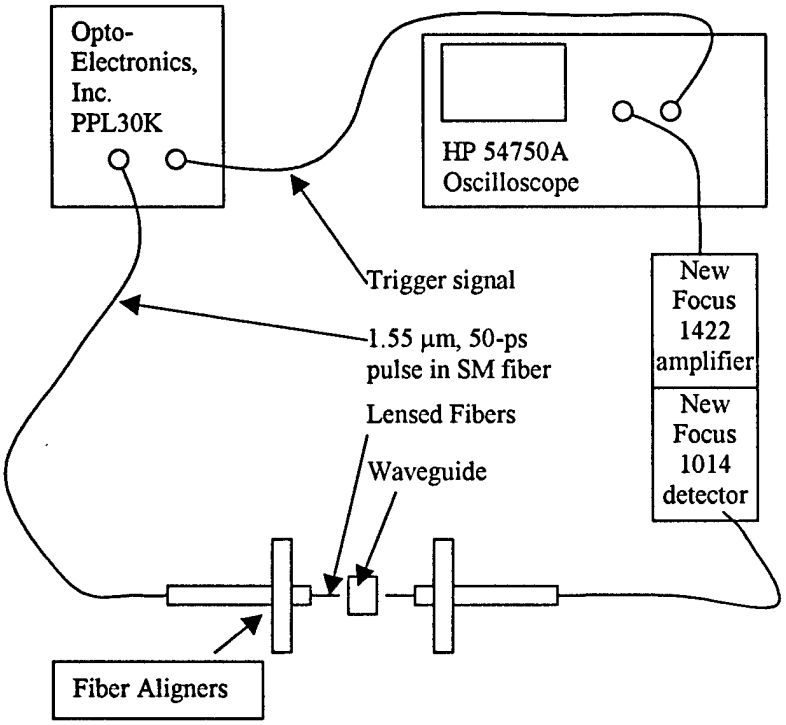


*Figure 19 : Experimental test set-up for measuring waveguide loss.*

The data from this set of experiments is summarized in Table 3. The waveguide number refers to the waveguides in Figure 13 with number 1 starting at the top. The suffix "a" refers to the thinner piece and "b" to the thicker piece. "Pa" refers to the typical completely passive waveguide on piece "a", and "Pb" refers to the typical passive waveguide on piece "b". "Thru" refers to the pulse height that would be achieved by coupling the two fibers directly. 60× attenuation was inserted before performing this measurement so photodiode saturation wouldn't be an issue.

Several problems were encountered in these experiments. High insertion loss overall meant that scattered light collected by the fiber was a significant source of error for some waveguides. It was possible to transmit a 5 mV pulse where there was no waveguide at all. Sometimes the signal would even be higher on adjacent waveguides than on the one being tested. High insertion loss draws waveguide numbers 1 and 2 into question and makes 8 unusable. The other major problem was poor waveguide yield. This experiment depends on adjacent waveguides being essentially the same with only one parameter

changed. Our waveguide process was sufficiently immature that some waveguides weren't even continuous from edge to edge. This reduced the number of usable test sites to those summarized in Table 3.

*Table 3 : Sumary of insertion-loss data for the various waveguide test structures.*

| WG# | Active sections per cell | Length of active section | Number of cells | Transmitted pulse height, mV | Modeled pulse height, mV |
|---|---|---|---|---|---|
| 1a | 1 | 40 | 8 | 4.5 | 3 |
| 2a | 2 | 20 | 7.5 | 4.5 | 3 |
| 3a | 1 | 20 | 8 | 19 | 25 |
| 4a | 2 | 10 | 7.5 | 26 | 27 |
| 5a | 1 | 10 | 8 | 54 | 76 |
| 6a | 1 | 20 | 8 | 27 | 25 |
| 7a | 1 | 30 | 8 | 9 | 8 |
| 8a | 1 | 40 | 8 | 0 | 3 |
| Pa | 0 | 0 | 8 | 175 | |
| Pb | 0 | 0 | 19 | 90 | |
| thru | | | | | 5400 |

The modeled numbers reported in Table 3 are based on a simple model that facilitates comparison. It assumes that assumes the following form for insertion loss:

$$IL = A\eta^N e^{-l_p\alpha_p - l_a\alpha_a},$$

where $A$ is a scale factor to account for fiber coupling loss at both facets, $\eta$ is the active-passive mode mismatch loss per active section, $N$ is the number of active sections, $l_p$ and $\alpha_p$ are the total length and absorption of the passive waveguide, and $l_a$ and $\alpha_a$ are the total length and absorption per unit length of the active waveguide. Although there are a large number of free parameters and significant scatter in the data, it is possible to find a set of parameters that match the data with fair accuracy. These parameters are summarized in Table 4. The most significant discrepancy between the BPM result and the measured result is the loss of the passive waveguide. The high loss could be due to a ridge etch that was too shallow, or from waviness of the ridges resulting from the wet etch process. The passive waveguide loss adds about 5% to the loss per section of the VMDP.

*Table 4 : Summary of waveguide parameters.*

| | BPM prediction | Fitted parameter |
|---|---|---|
| $\eta$ | 0.95 | 0.95 |
| A | N/A | 0.065 |
| $\alpha_a$ ($\mu m^{-1}$) | 0.0093 | 0.014 |
| $\alpha_p$ ($\mu m^{-1}$) | ~ 0 | 0.00022 |

### *Measurement of Integrated Photodetector*

After finishing the remaining mask steps to define the photodiodes, we tested the current-voltage (I-V) characteristics of each device prior to impulse response testing. We found that the vast majority of the devices failed I-V test. The primary reason was that the ridge etch and mesa etch undercut the etch masks in the region of the Schottky diodes. This was probably due to the non-planarity of the surface near the photodiode mesa. The etch undercut reduced the area available for the Schottky contact and made it likely that the Schottky metal would be touching InGaAs at some point. Without the barrier enhancement layer, the device is essentially a resistor. Fortunately, there were eight devices on the wafer that did not have this problem. Of these, three had significant optical response. The limiting mechanism here were the facet cleaves. With such a limited selection of devices, we were not able to discern "typical" behavior. We only have data on the two devices that worked, only one of which was the baseline design.

We tested the working samples with the PPL30K1.55 μm source used previously for passive waveguide testing and with a Time-Bandwidth Products 1.06 μm 150 fs pulsed laser. The response of a reference detector and the VMDP sample to the PPL30K is shown in Figure 20. The VMDP has a response about 7.5× lower than the reference New Focus model 1014 detector which has about 0.4 A/W. Using the $A$ parameter from Table 4, we can account for $A^{-1/2}$, or a factor of 3.9. Also, the pulse height will be lower by the ratio of the pulse widths. This VMDP sample had long tails in its response. The other working samples had cleaner pulses but lower response.

To get a better understanding of the impulse response of this structure, we switched to the shorter pulse of the 1.06-μm laser. The optical waveguide is absorbing at this wavelength, but if we are not concerned about responsivity, the wavelength can still be used. We illuminated the detector at a slight angle from the edge to strike the first photodiode from below. We detected the signal at the input and at the output of the VMDP. Since we are only illuminating one diode, it doesn't make that much difference which side we call the output.

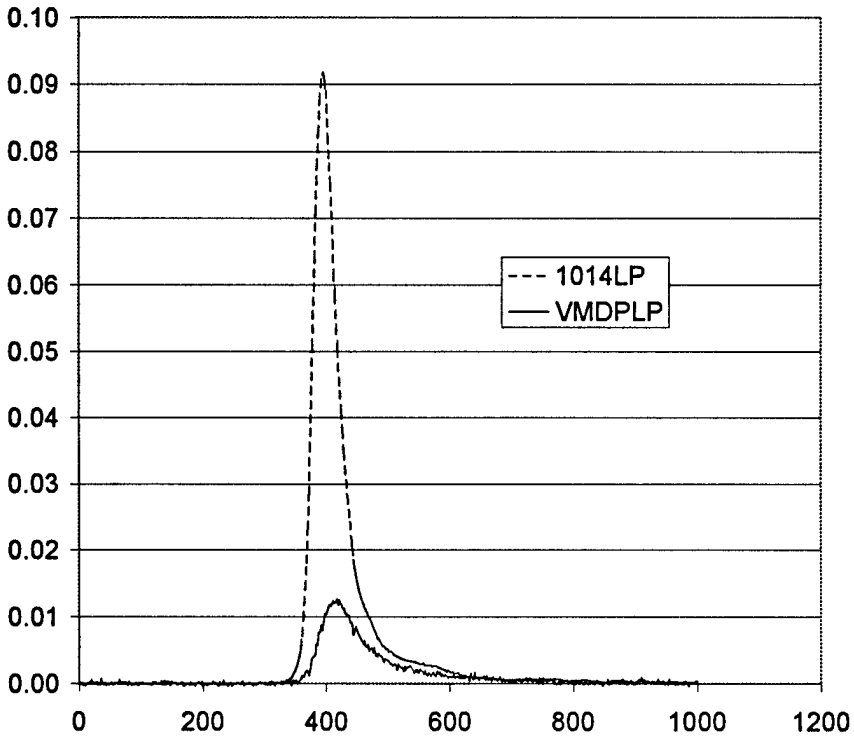


*Figure 20 : Response of the New Focus model 1014 and the VMDP photodiode to the PSP30K laser. The 1014 has 0.4 A/W responsivity so the VMDP is about 0.05 A/W. The low response of the VMDP is due to fiber coupling and tails in the pulse response of the VMDP.*

The response to the 1.06-μm illumination is shown in Figure 21. The probe at the far end of the line was lifted to provide a reflection at the end of VMDP. This reflection provides an easy means to measure the electrical length of the VMDP. The separation between the peaks is 27.3ps. To understand how this relates to the VMDP electrical parameters, we constructed a simple PSpice model for electrical simulation. The PSpice model showed best agreement with the 27ps peak separation for a diode capacitance of 18fF. This is in good agreement with the design value of 20 fF.

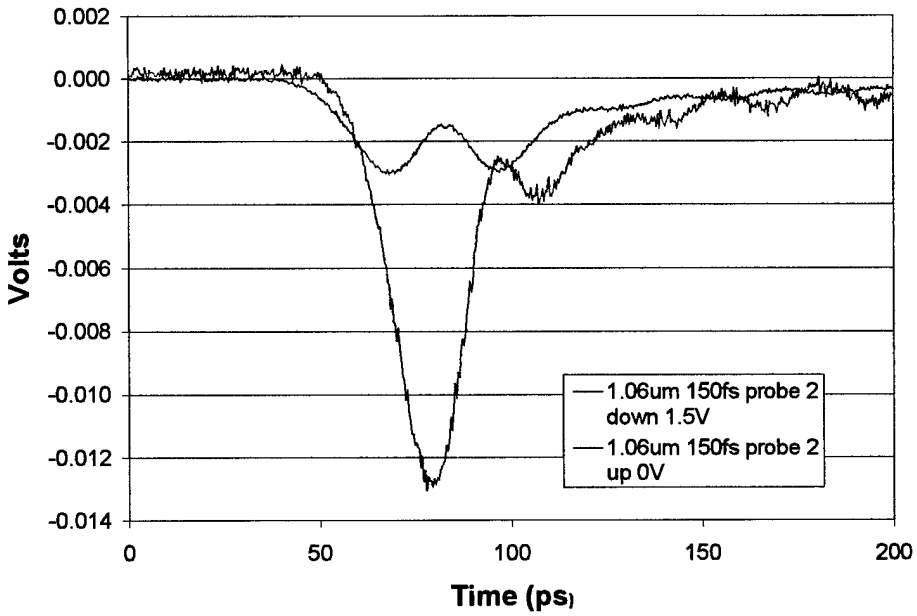


*Figure 21 : Impulse response of single diode in a 7-diode VMDP by illumination from edege at a slight upward angle. The distance between peaks is 27 ps.*

At this point, we sent the sample to Ming Wu's group at UCLA. They measured the frequency response of the detector using an optical heterodyne technique at 1.55 μm. They measured a 3-dB electrical bandwidth near 22 GHz. This was a surprising result considering that the design goal was 100 GHz. Reviewing the possible sources of performance loss, we noticed that an error was made in the layout of the ohmic contact to the photodiode elements. The design assumed a total ohmic-Schottky separation of 3-μm. The device was actually drawn with 22-μm separation. The extra separation increases the N+ series resistance from 7.56 ohms to 50 Ω.

PSpice simulations showed that the increase in resistance completely accounted for the lower than expected bandwidth. A properly drawn diode should achieve the design goal of 100 GHz.

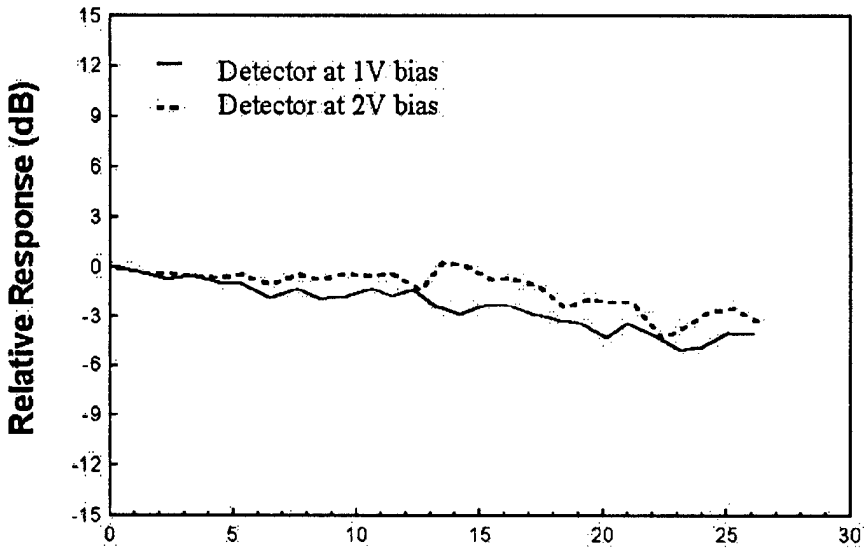


*Figure 22 : Frequency response of the VMDP sample measured by optical heterodyne technique.*

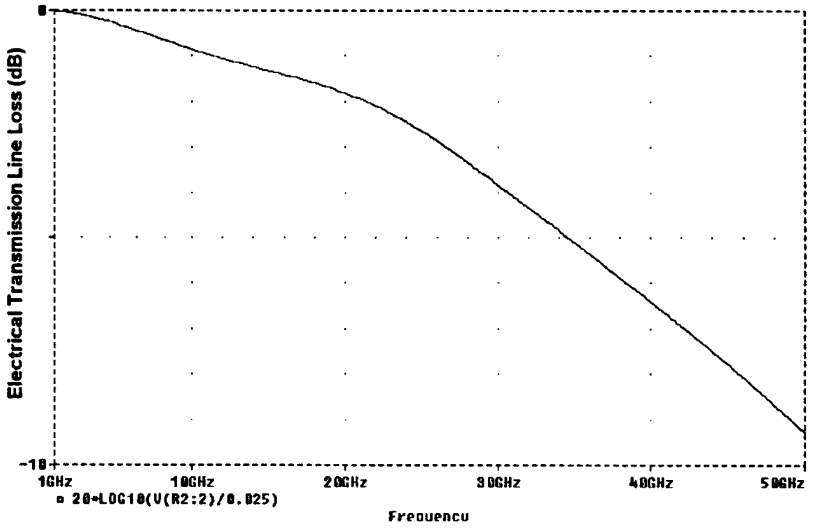


*Figure 23: Electrical transmission line loss.*

### *Measure New Focus Diode Saturation*

Keith Williams at the Naval Research Lab (NRL) measured the 1-dB small signal compression at 10 GHz. The compression current was up to 15 mA for the NF model 143X (detector area 300 $\mu m^2$) and up to 1 mA for the model 101X (detector area 100 $\mu m^2$). The model 101X has 3x less area than the 143X and half the intrinsic layer thickness. This does not account for the full difference between these models. We think that the early compression is due to the larger extrinsic mesa size of the model 1014. Carriers generated in the extrinsic mesa area will see a low electric field that will collapse at a lower photocurrent. The VMDP diodes have a very small extrinsic mesa and so would not suffer from this problem. The 15 mA would scale to 2 mA for the 40-$\mu m^2$ VMDP diodes. The thinner epitaxial layer of the VMDP (0.2 $\mu m^2$ compared with 1.0 for

the 1434) should provide an increase of a factor of 5 since the space charge field is integrated over a smaller distance. The net result is that we expect the VMDP to have about the same saturation current or slightly more than the 1434's 15 mA.

### *Measure Electrical Waveguide Properties*

To understand the impact of having a strip of conducting material running down the center of the electrical waveguide, we designed coplanar-strip electrical transmission lines with conducting strips of 0, 5, and 10 μm width. These test structures were fabricated on GaAs before we received the InP based materials. The devices were measured up to 50 GHz by Prof. Wu's group. No measurable difference in microwave loss was found between the structures. The overall loss in each case was less than 1 dB at 50 GHz. The test structures are shown in Figure 24

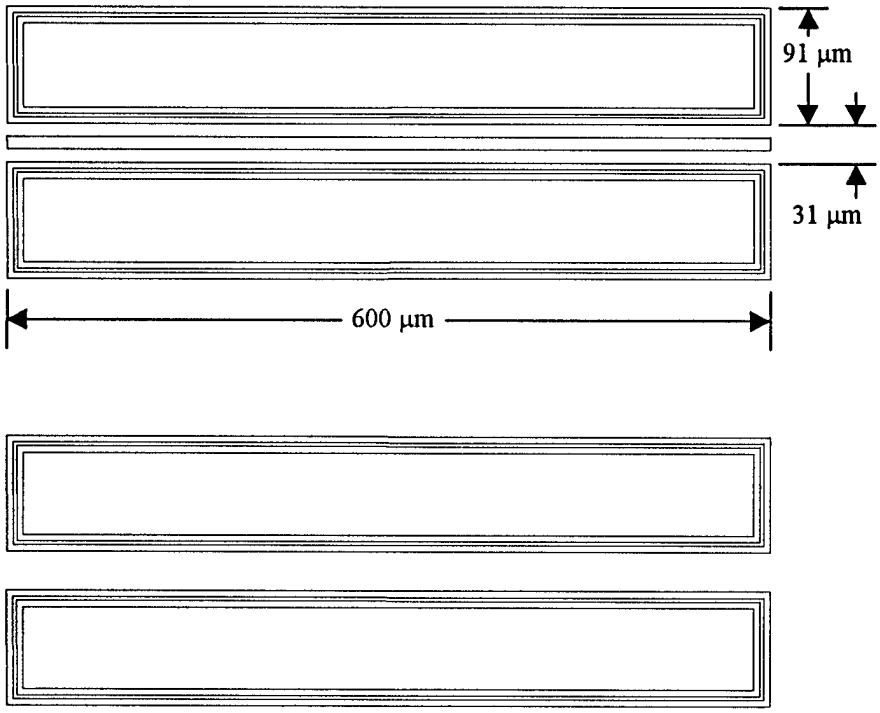


*Figure 24 : Layout of test structure to evaluate effect of a doped strip of semiconductor running down the center of the electrical guide. Structures were fabricated with 0, 5, and 10 μm doped strip width.*

### *Design New Electrical Waveguide*

Some of the concepts of distributed amplification first described in detail by Ginzton, *et. al.* [3] are directly transferable to the VMDP. The optical waveguide replaces the vacuum-tube-grid-loaded input transmission line and the photodiode connections on the output transmission line replace those of the vacuum-tube plate. Actually, the VMDP is not fully analogous to the distributed amplifier since no attempt is made to incorporate the optical waveguide discontinuities created by the photodiode structures into the design of the optical waveguide. There are no significant frequency dependent losses on the "grid" line of the VMDP. Another difference is that transmission-line sections are used in place of inductors in the design of the output line. These differences prevent the complete

incorporation of Ginzton's recommendations for improved frequency response. However, there is at least one very significant recommendation from this paper that does appear to apply design to the case of VMDPs: how to handle impedance transformation.

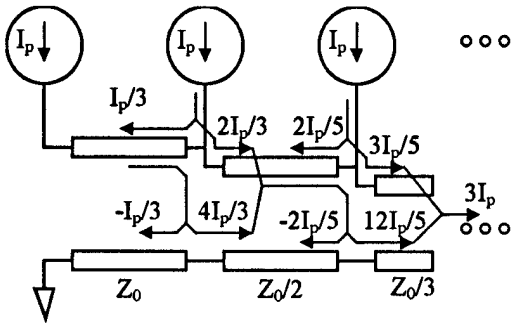


*Figure 25: Illustration of how current sources can be connected along a transmission line with no termination on one end so that the currents add at the terminated output. The minus signs in the figure are correct for nodal analysis, not wave amplitude (after Ginzton).*

The trick is to step-wise taper the transmission line impedance from the input to the output of the output line. Reflections generated at each impedance step are made to exactly cancel by suitable choice of section impedance. The technique is illustrated in Figure 25 for the particular case of an open circuit for the input termination. The first current source on the unterminated end will source all of its current, $I_p$, into the line section $Z_0$. When this wave reaches the next line section, $Z_0/2$, the current reflection coefficient will be -1/3 and the transmission coefficient, 4/3. The second current source will split its current between the two sections based on the relative impedances. One third of the current will travel toward the input and 2/3 toward the output. The 1/3 exactly cancels the –1/3 from the reflected incident wave while the 2/3 adds with the transmitted wave for a full $2I_p$. The process is repeated at the next current source, for a suitable choice of line impedance, $Z_0/3$. In general,

$$Z_{n+1} = Z_n\left(\frac{n}{n+1}\right)$$

starting with an arbitrary $Z_1$.

This theory can be easily generalized for the case where the various currents are not equal in magnitude. The general rule is that at each section,

$$z_m = \frac{1}{1+i_m},$$

where $z_m$ is the ratio $Z_{n+1}/Z_n$ and

$$i_m = \frac{I_{n+1}}{\sum_{k=1}^{n} I_k}.$$

We used Orcad PSPICE to quickly simulate this structure to see if there are any hidden problems with this approach. The circuit diagram is shown in Figure 26. Spice

simulations confirmed that this structure has frequency-independent response and 100% efficiency.

This concept lends itself particularly well to the case of the VMDP. In this case, it is easy to adjust the section impedance by simply making the photodiode larger. In addition, the larger photodiodes are toward the output, which is desirable for uniform optical absorption as well. Further adjustment of section impedance can be achieved by adjusting the line impedance that connects the photodiodes.

However, there is a practical limit to this approach. Unwanted reactance makes it difficult to achieve perfect cancellation of the reflected waves over a broad range of frequencies. In addition, there is a practical limit to the range of section impedances that can be achieved. Given that the photodiode equivalent circuit is much simpler than any gain element, it seems reasonable to expect that the task will be easier for the case of the VMDP than for the distributed amplifier.

To investigate the unterminated VMDP we developed a Spice model that incorporates the delays and losses of optical waveguide, and varying absorption, capacitance, and resistance for the photodiode elements. The schematic is shown in Figure 27. Again there are two sections of the schematic: lower and upper. The lower section represents the optical waveguide while the upper sections represents the electrical waveguide. Voltage is used as the stand-in for optical intensity. This Spice package includes idealized multipliers that are shown on the schematic as the symbol ⊗. These multipliers perform a mathematical multiplication of the voltages at the input and provide the product as a voltage at the output. The multipliers and batteries are not physical. We used them to model the effects of optical waveguide loss (multiplying by the fractional loss) and absorption (multiplying by the fractional absorption). We used batteries to generate the input numbers for the multiplier.

We used conductance blocks to represent the photodiode action. This block converts a voltage (which represents optical intensity in the lower half of the schematic) to a current on the electrical transmission line. Each conductance block has a conductance of 1.0 because the incomplete optical absorption is separately modeled with a multiplier before the conductance block. Photodiode capacitance and series resistance are modeled in the usual way. We made an attempt to build scaling into this model by assuming that photodiode absorption and capacitance are proportional to photodiode length while series resistance is inversely proportional to length. Since absorption is actually exponential with length, this scaling rule will overestimate capacitance and underestimate resistance for larger absorption.

The results of the simulations are shown in Figure 28 through Figure 31. It is unlikely that we have hit on the optimum unterminated VMDP design, but the results do show that this approach has good promise. The first results in Figure 28 and Figure 29 we show what would happen with a uniform VMDP with no input termination. The drastic frequency response ripple and poor step-response show why this is generally not done. Figure 30 and Figure 31 however, illustrate that proper choice of transmission line impedance and photodiode size can result in acceptable performance with double the efficiency achievable when using an input termination.

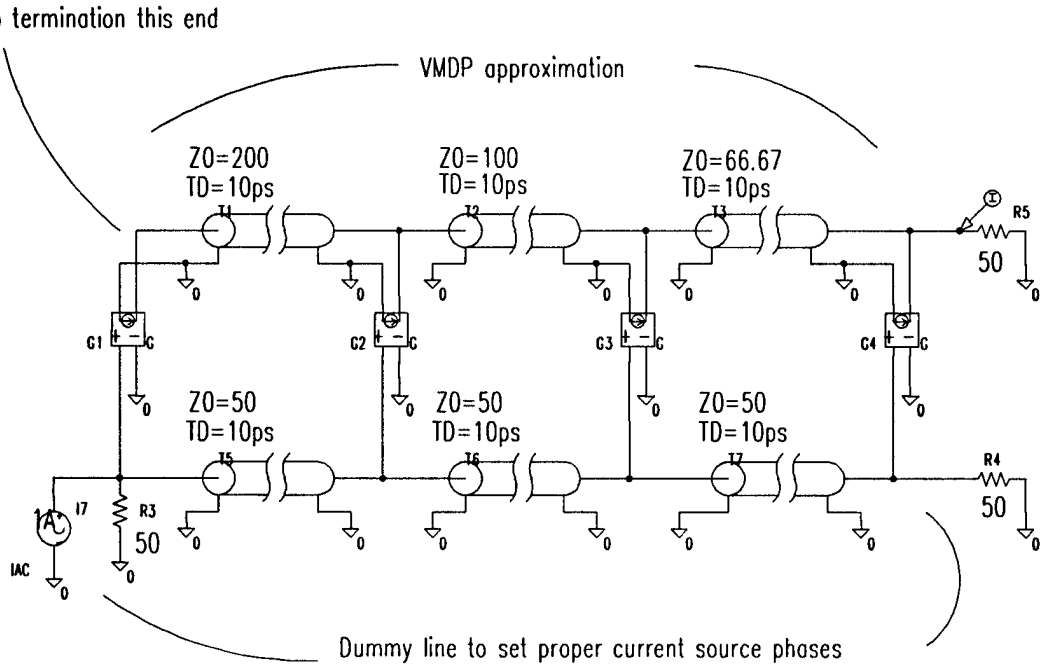


*Figure 26: Simple model to test Ginzton approach to no termination on distrubuted current source line.*

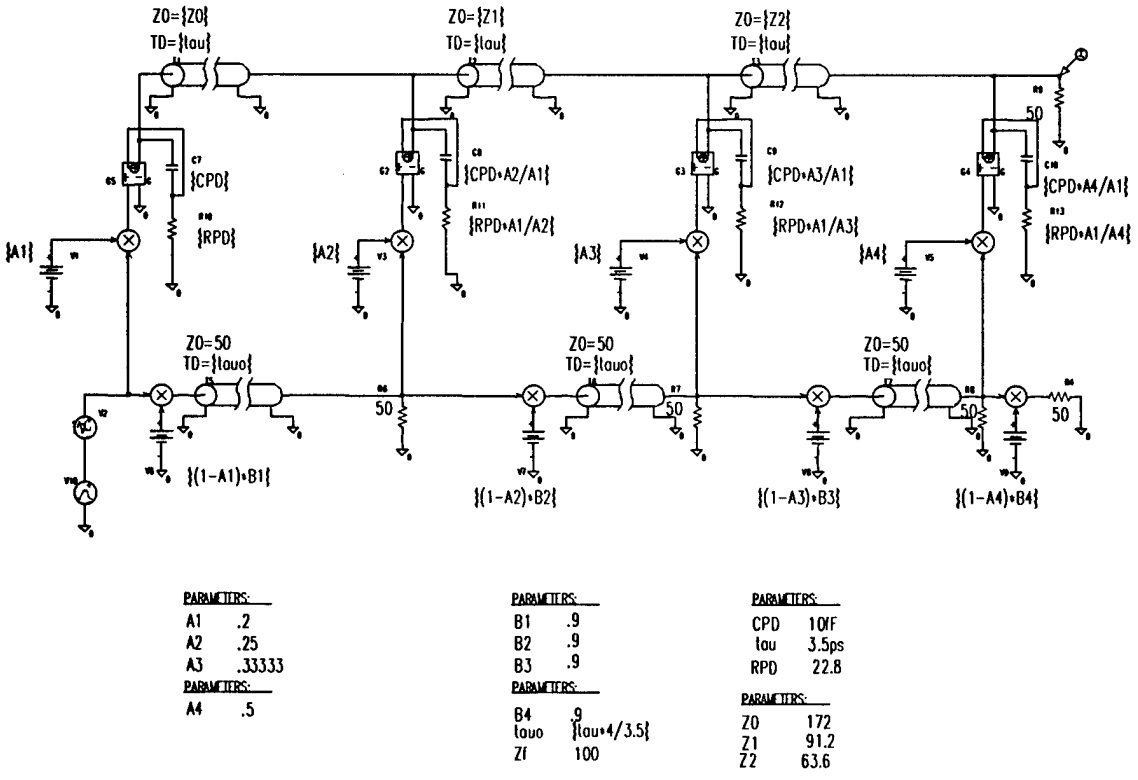


*Figure 27 : Four diode unterminated VMDP structure used in simulations. The upper transmission line sections represent the electrical transmission line, the lower ones, the optical waveguide.*

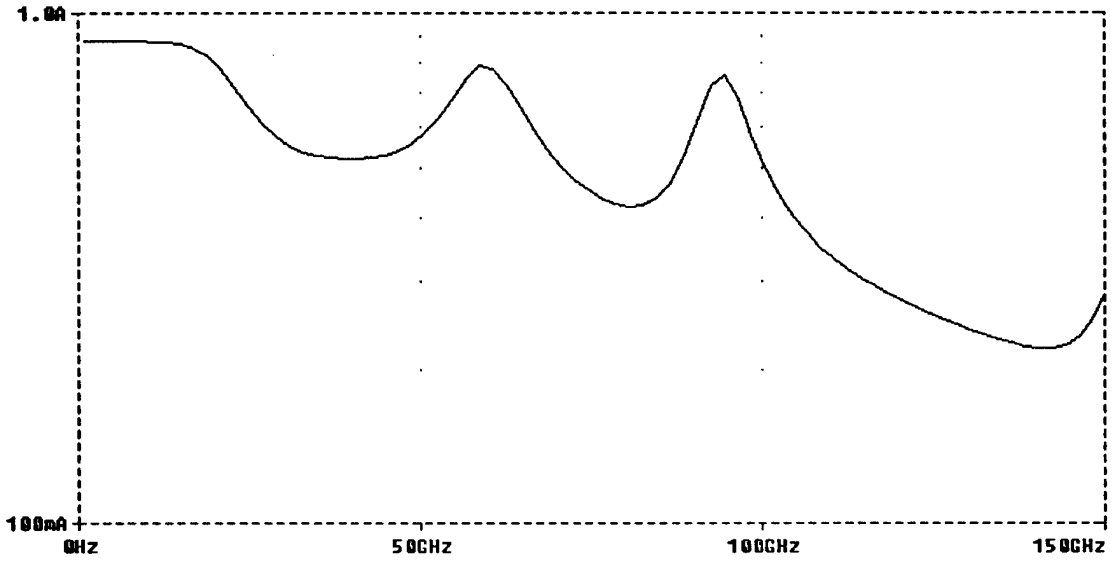


*Figure 28 : Frequency response of a uniform VMDP with no input termination. Frequency response ripple is greater than 6 dB. Parameters used for simulation: Z1- Z3=100Ω, B1-B4=1.0, A1=.22, A2=.282, A3=.393, A4=0.647.*

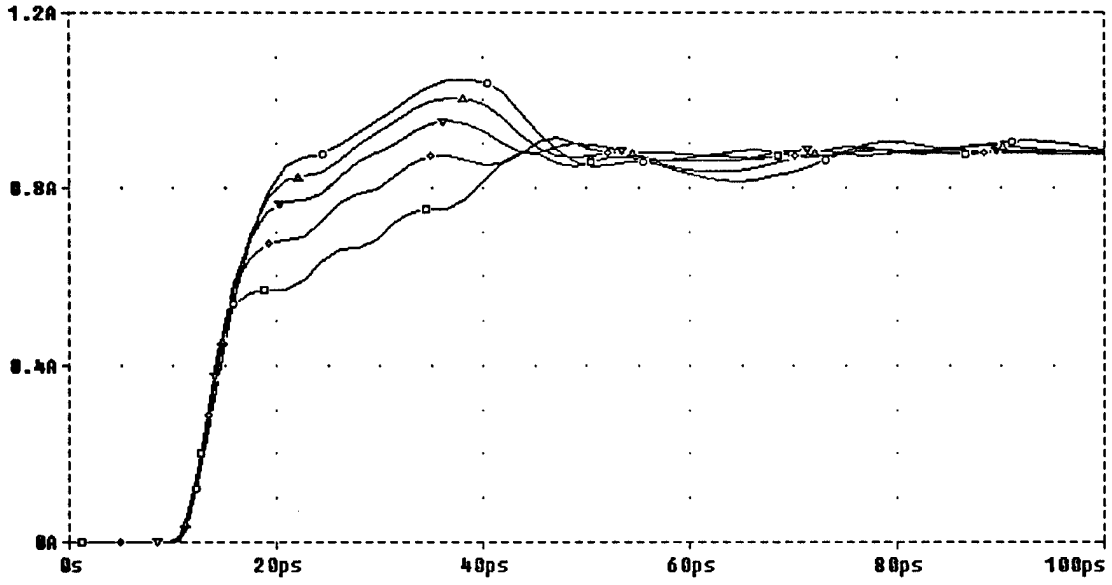


*Figure 29 : Step response of the unterminated uniform VMDP structure. Curves are for transmissio line impedance ranging from 50 to 150 ohm. No value provides a flat response. Parameters used for simulation: Z1- Z3=100Ω, B1-B4=1.0, A1=.22, A2=.282, A3=.393, A4=0.647.*

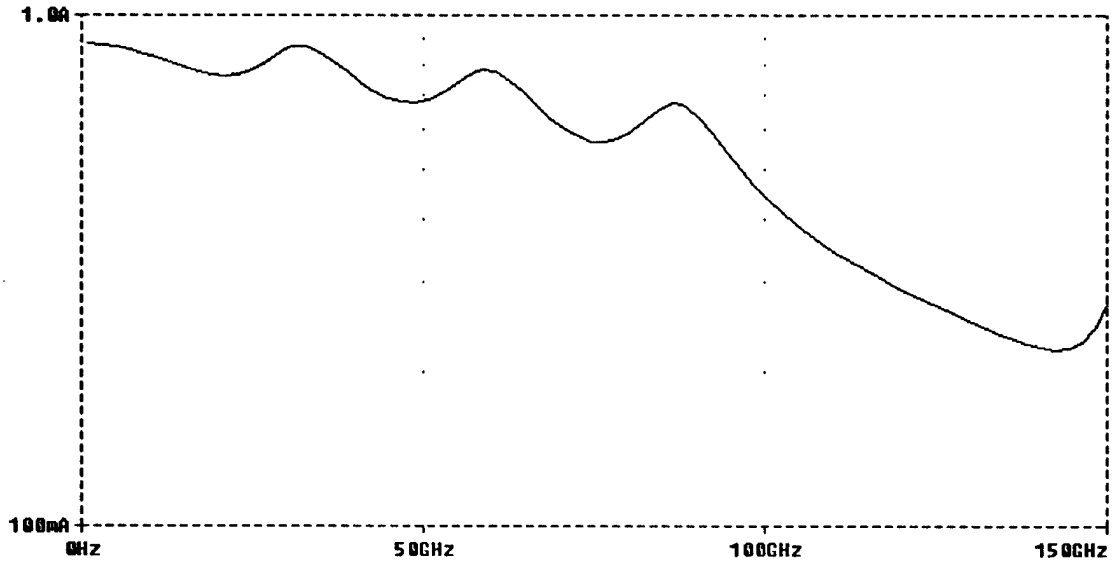


*Figure 30 : Frequency reponse of the unterminated VMDP using the Ginzton approach to cancel backward waves. Frequency response ripple generated by imperfect cancelation is 3 dB peak to peak. Parameters used for simulation: Z1- Z3=200Ω,100Ω, 66.67Ω; B1-B4=1.0; A1- A4= 0.22, 0.282, 0.393, 0.647.*

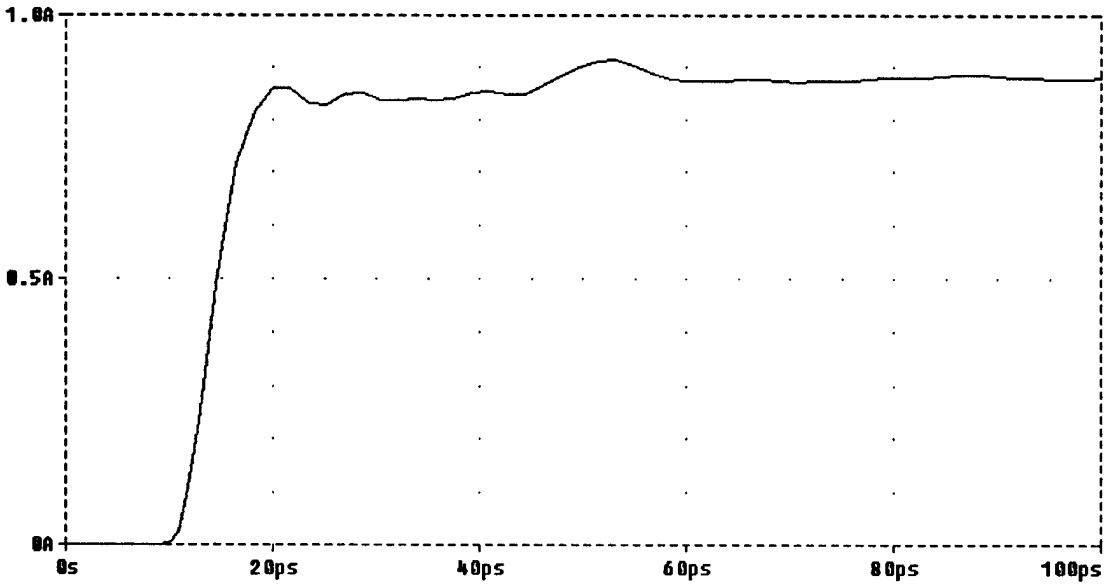


*Figure 31 : Step response of the unterminated VMDP using backward-wave cancelation. Note that the step respone achieves more of it's full value in the first transition without significant overshoot or ringing. Parameters used for simulation: Z1- Z3=200Ω, 100Ω, 66.67Ω; B1-B4=1.0; A1- A4= 0.22, 0.282, 0.393, 0.647.*

# Recommendations

This work has shown that Schottky diodes can be integrated with an optical waveguide and that the VMDP structure can achieve efficiencies well over 50% approaching 90%. This structure needs further investigation to resolve problems with poor fiber coupling efficiency, optical waveguide loss, and photodiode yield. We feel that all of these issues can be resolved with more effort. Given the importance of high-power photodiodes for RF-photonic applications including phased-array antenna distribution and optical A/D conversion, we recommend that this effort be funded into Phase II. The devices resulting from the Phase II effort would provide a factor of ten increase in optical power handling capability and a factor of two increase in speed over existing devices.

# References


1 L.Y. Lin, *High-Powered, High-Speed Photodetectors and Micromachined Free-Space Integrated Optics*, UCLA PhD Thesis, 1996.

2 A. Sneh, J.E. Zucker, and B.I. Miller, "Compact, Low-Crosstalk, and Low-Propagation-Loss Quantum-Well Y-Branch Switches," *IEEE Photon. Technol. Lett.*, vol. 8, no. 12, pp. 1644-1646, 1996.

3 Ginzton, Hewlett, Jasberg, and Noe, "Distributed Amplification," *Proc. IRE*, 1948, pp. 956-969.